2021-01-1147 Published 21 Sep 2021

Modeling the Effects of the Ignition System on the CCV of Ultra-Lean SI Engines using a CFD RANS Approach

Lorenzo Sforza, Tommaso Lucchini, and Gianluca Montenegro Politecnico di Milano

Cagdas Aksu and Taisuke Shiraishi Nissan Motor Co Ltd

Citation: Sforza, L., Lucchini, T., Montenegro, G., Aksu, C. et al., "Modeling the Effects of the Ignition System on the CCV of Ultra-Lean SI Engines using a CFD RANS Approach," SAE Technical Paper 2021-01-1147, 2021, doi:10.4271/2021-01-1147.

Abstract

Cycle-To-Cycle Variability (CCV) must be properly considered when modeling the ignition process in SI engines operating with ultra-lean mixtures. In this work, a strategy to model the impact of the ignition type on the CCV was developed using the RANS approach for turbulence modelling, performing multi-cycle simulations for the power-cycle only. The spark-discharge was modelled through a set of Lagrangian particles, introduced along the sparkgap and interacting with the surrounding Eulerian gas flow. Then, at each discharge event, the velocity of each particle was modified with a zero-divergence perturbation of the velocity field with respect to average conditions. Finally, the particles velocity was evolved according to the Simplified Langevin Model (SLM), which keeps memory of the initial perturbation and applies a Wiener process to simulate the stochastic interaction of each channel particle with the surrounding gas flow. The particles diameter was also evolved, according to both the energy transfer from the electrodes and the local stretched laminar flame speed. The proposed methodology was assessed against experimental measurements from a pent-roof high-tumble single-cylinder SI engine, equipped with an electrical circuit able to provide both standard and enhanced discharge events. Promising results were achieved in terms of predicted IMEP and its CoV.

Introduction

The Spark-Ignition (SI) engine technology is currently under continuous improvement, in order to achieve, simultaneously, the maximum thermal efficiency as well as near-zero pollutant and green-house gases emissions [1, 2, 3, 4, 5, 6]. This high industrial and academical interest is justified by several aspects, such as the low cost, the high power-to-weight ratio and the fuel flexibility, which make SI engines as one of the most interesting and feasible solutions towards a complete decarbonization of vehicles powertrain technology [7, 8, 9]. In this framework, combustion efficiency and control become fundamental at all conditions covered by the engine map [10, 11]. For example, at part-loads, the interest towards ultra-lean mixtures led to an increase of the combustion Cycle-To-Cycle Variability (CCV), due to the stochastic nature of turbulent flow structures interacting with a flame front which is easy to quench [12, 13]. Therefore, high CCV values are an important limiting factor for the SI engine design, because associated with potential knocking phenomena (lower thermal efficiency) [14, 15] and misfiring events (enhanced unburned hydrocarbon emissions) [13].

A contribution to combustion CCV is also provided by the evolution of the spark-discharge in presence of high gas flow velocities close to the ignition zone [13, 16]. In fact, if, from one side, this condition allows to inhibit early combustion fluctuations by shortening the ignition delay [17], on the other hand a strong flow can produce spark blowouts and channel restrikes (re-ignitions), limiting the ignition process [16, 18, 19, 20]. As a consequence, cycle-to-cycle spark formation may become unstable, causing a higher CCV in the early flame development [16]. A possible solution is represented by the use of enhanced coil types, which can generate stronger spark-discharges for longer durations [16, 19, 20, 21].

In the present work, a methodology to predict the effects of the coil features on the combustion CCV of a SI engine is proposed. The developed strategy is based on the RANS approach for turbulence description and on a comprehensive model architecture to handle the different phenomena involved. The ignition stage is simulated through a Lagrangian approach, in which particles are introduced along the spark-gap and interact with the surrounding Eulerian gas flow. At each discharge event, the channel velocity is homogeneously modified with a divergence-free perturbation with respect to average conditions. Then, the velocity of the channel particles is evolved according to a Simplified Langevin Model (SLM), which keeps memory of the initial perturbation and simulates, through the Wiener process, the stochastic diffusion generated by the random interactions of each particle with the molecules of the surrounding mixture. The particles diameters are also modified according to the heat provided by the electrical

circuit and the local laminar flame speed value. This last contribution makes the channel particles also markers of initial flame kernels. A pent-roof high-tumble single-cylinder SI engine, fueled with an ultra-lean (ϕ < 0.6) Isooctane-Air mixture, was selected for the assessment of the proposed methodology. At fixed engine conditions, a comparison between standard and enhanced coils was carried out. Numerical results from 20 independent single-cycle spark-discharges showed consistent trends in terms of IMEP and CCV variations with respect to experimental data measured over 200 power-cycles. This demonstrated how the proposed numerical approach seems very promising for a preliminary estimation of the impact of the flame kernel growth process on combustion stability.

Numerical Models

A strategy based on a *multi-physics modeling approach* is selected to handle the interplay between all complex phenomena involved in a premixed SI combustion event. In particular, a *coupled Lagrangian-Eulerian* approach is chosen for the simulation of the ignition stage and the following initial flame development. Instead, the turbulent flame propagation is modelled with an *Eulerian-only* strategy.

Spark-Channel Model

The spark-channel evolution is predicted by the use of *Lagrangian particles*, whose aim is to simulate the ignition event with a trade-off between a high accuracy level and low computational costs. At the ignition event, along the spark-gap centerline, a user-defined number of particles is introduced. Their temperature T_p and diameter d_p are initialized as function of the breakdown stage features [22, 23, 24, 25], because only arc and glow stages of the spark-discharge are modelled in this work. Then, each particle, which represents a portion of the spark-channel and a possible ignited flame kernel, is evolved in terms of *position* and *dimension*. This is performed according to: the surrounding flow and mixture conditions, the heat available inside the channel after the breakdown stage and the electrical circuit support. In case two particles become too far from each other, the continuity of the channel and its shape consistency with the velocity field are guaranteed by a dynamic introduction of a new particle, whose initial properties (position, temperature, diameter and velocity) are averaged from the previous two particles.

Particle tracking To simulate the CCV of the spark-channel spatial evolution, at each discharge event:

1. first, an initial perturbation $\mathbf{U}_{rnd}$ is homogeneously applied to the velocity of all channel particles;
2. then, the velocity of each particle $\mathbf{U}_{p,(t)}$ is evolved according to stochastic differential equations.

The aim of the initial perturbation $\mathbf{U}_{rnd}$ is to mimic a random variation, with respect to average conditions, of the velocity field experienced by the early spark-channel

$$\mathbf{U}_{p,(t=0)} = \tilde{\mathbf{U}} + \mathbf{U}_{rnd} \tag{1}$$

In particular, for consistency reasons with the average fields and the physical aspects of turbulence, the $\mathbf{U}_{rnd}$ vector, whose components are stochastic independent variables with a Gaussian distribution of zero-mean and u' standard deviation, is homogeneously applied to all channel particles to simulate a zero-divergence perturbation. Afterwards, the velocity of each particle is evolved, keeping memory of the initial perturbation, as

$$\mathbf{U}_{p,(t;t>0)} = \mathbf{U}_{p,(t-dt)} + d\mathbf{U}_p \tag{2}$$

where the velocity variation $d\mathbf{U}_p$ is computed through the stochastic differential equations of the Langevin model [26]. This approach allows to simulate, starting from mean Eulerian flow quantities, the variation of a Lagrangian particle velocity according to the stochastic diffusion process generated by its random interactions with the molecules of the surrounding mixture [26, 27]. In this work, as a first step, the Simplified version of the Langevin Model (SLM) [26, 28, 29] is used

$$dU_{p,i} = \left(g_i - \frac{1}{\bar{\rho}} \frac{\partial \tilde{p}}{\partial x_i} \right) dt + G\left(U_{p,i} - \tilde{U}_i \right) dt + C_0 \varepsilon^{1/2} dW_i \tag{3}$$

where, along each spatial direction $i = x, y, z$, the variation of a particle velocity $dU_{p,i}$ is function of: the gravitational acceleration g_i and the mean pressure gradient $\partial\tilde{p}/\partial x_i$ (first RHS term), the difference between the particle $U_{p,i}$ and the mean flow $\tilde{U}_i$ velocities (second RHS term), the Wiener process dW_i (third RHS term). This last term can be approximated as follows [26]

$$dW_i = \eta_i dt^{1/2} \tag{4}$$

in which η_i is one of the three independent standardized Gaussian random variables of the vector η. Because the last RHS term of Eq. 3 simulates a random walk of the particle in the velocity space, the coefficent $C_0\varepsilon^{1/2}$ must be independent from dW_i to maintain the Markovian nature of the system [26]. In particular, C_0 should be a universal constant in the high-Reynolds-number limit [30, 31] with a value of C_0= 2.1 [32], while ε is the turbulence kinetic energy dissipation rate of the average flow field. Moreover, it is worth to mention that, thanks to SLM approach, the G parameter of Eq. 3 is not a tensor but a coefficient, equal along all spatial directions to

$$G = -\left(\frac{1}{2} + \frac{3}{4} C_0 \right) \omega \tag{5}$$

being $\omega = \varepsilon/k$, with k as the turbulent kinetic energy. Therefore, the position of each particle x_p representing a portion of the spark-channel can be computed according to

$$\mathrm{x}_{p,(t;t>0)} = \mathrm{x}_{p,(t-dt)} + \mathbf{U}_{p,(t-dt)} dt \tag{6}$$

Particle size evolution The temporal evolution of the spark-channel diameter is simulated, locally, through the variation of each particle dimension, considering:

1. the heat available inside the channel after the break-down stage;
2. the electrical circuit support;
3. the early laminar flame stage.

This last contribution, which makes the channel particles also markers of initial flame kernels, is here included because the Lagrangian approach allows a flexible and grid-independent modeling of the early laminar flame development. Some examples can be the possibility of estimating the local laminar flame stretch as function of each kernel curvature [33], as well as the tracking of early flames generated by spark-channels whose electrical circuit support is vanished before the achievement of a fully-developed turbulent stage. Similarly to [34, 25], for each particle, both mass m_p conservation and radius r_p variation equations are solved

$$\frac{dm_p}{dt} = 4\pi r_p^2 \rho_u \left(s_{lam} + \frac{\rho_p}{\rho_u} s_{plasma} \right) \tag{7}$$

$$\frac{dr_p}{dt} = s_{plasma} + s_{therm} + \frac{\rho_u}{\rho_b} s_{lam} \tag{8}$$

being ρ_p the particle density, while ρ_u and ρ_b the unburned and burned mixture densities at particle position. The effect of an initial fast expansion of the channel, due to the heat available inside the arc after the breakdown event, is modelled through s_{plasma} (see both Eqs. 7 and 8). As performed in [34, 25], a dedicated submodel estimates the s_{plasma} value through an heat conduction equation applied to a 1D axisymmetric mesh, representing a wedge of the gas region around the spark-gap centerline. The influence of the electrical circuit, which continuously provides heat during the channel evolution, is considered via s_{therm} (see Eq. 8), which could be modelled as function of the particle temperature variation dT_p/dt (Eq. 9), computed from the energy conservation equation of the particle itself (Eq. 10) [34, 25]

$$s_{therm} = \frac{V_p}{A_p} \left(\frac{1}{T_p} \frac{dT_p}{dt} - \frac{1}{p} \frac{dp}{dt} \right) \tag{9}$$

$$\frac{dT_p}{dt} = -\frac{\dot{m}_p}{m_p} \left(T_p - T_{ad} \right) + \frac{\dot{Q}_{spk} \eta_{eff}}{m_p c_p} + \frac{1}{\rho_p c_p} \frac{dp}{dt} \tag{10}$$

where c_p is the specific heat and $\dot{Q}_{spk}\eta_{eff}$ the net thermal energy provided by the electrical circuit. This last contribution is estimated by a suitable electrical circuit sub-model, as described in the next section. The effect of the early laminar flame development is included by computing the actual laminar flame speed s_{lam}

$$s_{lam} = I_0 \, s_{u,lam} \tag{11}$$

as function of its unstrained value $s_{u,lam}$, estimated with the correlation proposed by Gulder [35], and the flame stretch I_0. In this work, the empirical correlation proposed by Bray [36]

$$I_0 = \frac{C}{1+\tau} K^{-0.784} \tag{12}$$

is selected for the I_0 value computation, where $C = 0.467$, τ is computed as function of the burned T_b and unburned T_u mixture temperatures at particle position

$$\tau = \frac{T_b}{T_u} - 1 \tag{13}$$

while K is the Karlovitz number according to [37]

$$K = 0.145 \left(\frac{u'}{s_{u,lam}} \right)^2 \mathrm{Re}_L^{-0.5} \tag{14}$$

It is worth to mention that Bray's correlation (Eq. 12) was extracted from experimental data of turbulent flames only [36] and does not include the modelling of the laminar flame thermo-diffusive instability (no dependency on Markstein length), which here, as a first step, is neglected. However, it allows to properly predict the quenching effects produced by extremely high levels of turbulence on the flame. This becomes extremely important especially when high flow velocities, and connected high turbulence intensity levels, are generated near the ignition zone. In fact, as reported in [16], to ignite ultra-lean mixtures an increase of the gas flow velocity at the ignition position is usually adopted to inhibit the early combustion fluctuations by shortening the initial stage of combustion. Therefore, Eq. 12 is adopted on both this Lagrangian approach and the further Eulerian turbulent flame development, where it can be still applied. As shown by Figure 1, if the maximum I_0 value computed from Bray's correlation is limited to 1 (no stretch), Eq. 12 is well suited to model the stretch effects generated by a high level of turbulence, because of its dependency on Karlovitz number (Eq. 14).

Electrical circuit model A detailed model of a classical inductive ignition system is adopted in this work to consider with a satisfactory accuracy the effects produced by different coil types on the ignition process. The approach proposed in [25] was followed, therefore only the secondary circuit is modelled in detail, taking into account its resistance R_S. The inter-electrode voltage V_{Ie} is computed including the cathode V_{cf} and the anode V_{af} potential drops, as well as the gas column voltage fall

$$V_{gc} = a l_{spark} i_S^b p^c \tag{15}$$

FIGURE 1 Dependency of Bray's correlation for stretch (Eq. 12 with $C = 0.467$) on Karlovitz number (Eq. 14), assuming T_u and T_b equal to 300 K and 2000 K, respectively.

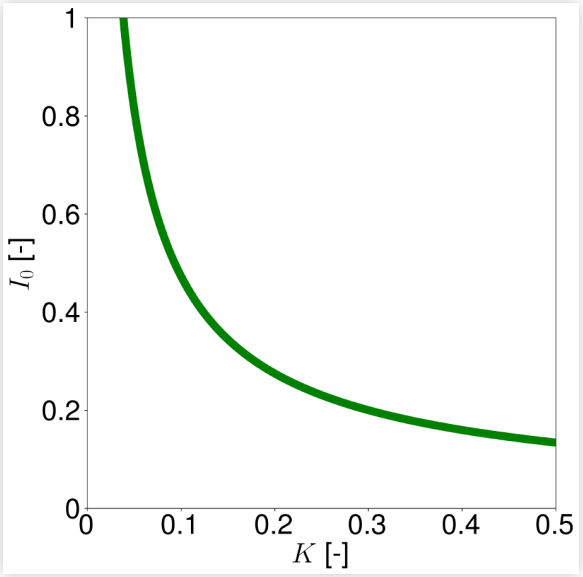

which depends on the temporal evolution of the secondary circuit current i_S, spark-channel length l_{spark} and pressure p. As suggested by [38], Eq. 15 coefficients a, b and c change when the discharge moves from arc to glow stage. The time-variation of the secondary circuit energy dE_S/dt is computed according to:

- the gross thermal power transferred to the spark-channel $\dot{Q}_{spk} = V_{IE}\, i_S$;
- the heat losses along the circuit $R_S^2\, i_S$ (Joule effect).

An estimation of the heat losses at the electrodes, in terms of efficiency η_{eff} of the energy transfer process to the gaseous mixture, is carried out following the approach of Herweg and Maly [39, 25].

Differently from [25], here the discharge profile in time of the secondary-circuit current $i_{S,(t)}$ can be directly provided to the model instead of the stored primary circuit energy. This allows a higher flexibility in the knowledge of the electrical circuit features, being the secondary current trend an easy-measurable magnitude. As a consequence, the related total energy stored inside the circuit can be estimated afterwards, when the discharge is completed.

Further details about secondary circuit modeling and related coefficients (e.g. a, b and c of Eq. 15) are provided in [25].

Restrike model Partial restrikes, as well as complete reignitions, are considered in this work, to mimic the behaviour of the spark-channel in a single power-cycle. An example of incomplete channel shortenings, also called *short circuit restrikes*, can be oserved in the work of Sayama [20]. Therefore, taking as physical basis the observations available in [40], the breakdown voltage V_{bd} is estimated with the following general expression

$$V_{bd,AB} = a_1 + b_1 \frac{p}{T_u} + c_1 \frac{p}{T_u} \left(\delta L_{AB}\right)^{n_1} \tag{16}$$

in which A and B are the two generic positions along the spark-channel where a shortening could happen, being δL_{AB} the minimum distance between them. Coefficients a_1, b_1, c_1 and n_1 are calibrated on experimental measurements of a single power-cycle, following the methodology used in [20]. As a consequence, any type of restrike event can be modelled between positions A and B if

$$V_{gc,AB} > V_{bd,AB} \tag{17}$$

where $V_{gc,AB}$ is the gas-columns voltage drop computed from Eq. 15 by using the distance between A and B inside the corrugated spark-channel $l_{spark,AB}$.

When a restrike event is detected, first a new set of Lagrangian particles is introduced along the minimum distance between positions A and B to represent the new spark-channel shape. The properties of the new particles, in terms of diameter, temperature and velocity, are computed by averaging the channel features in A and B. Then, the particles detached from the spark-channel are no more supported by the electrical circuit. Nevertheless, they are still evolved in terms of both position and dimension until a turbulent flame is generated, because representing possible ignited flame kernels.

Turbulent Combustion Model

The propagation of a self-sustained turbulent flame is predicted by using a classical *Eulerian* approach, based on the *flamelet* assumption: the Coherent Flame Model (CFM) [41, 42, 43, 44]. Thanks to its methodology for the flame-turbulence interaction modelling, which is based on the evolution of flame surface density Σ field, the CFM can be easily coupled with a Lagrangian ignition model. In fact, from the spatial distribution of Lagrangian particles, both the volume V_{spk} and the cylindrical surface S_{spk} of the spark-channel can be estimated. Therefore, the ignition system effects can be transferred to the 3D computational domain as

$$\Sigma_{ign} = \frac{S_{spk}}{V_{spk}} \tag{18}$$

where Σ_{ign} is an average flame surface density imposed by the channel over the occupied cells. Eq. 18 is valid not only for the arc sustained by the electrical circuit, but also for restriked channels. Since spark-timing, the reaction propagation on the Eulerian domain is solved by a transport equation for a combustion progress variable c [44, 43, 37]

$$\frac{\partial \rho \tilde{c}}{\partial t} + \nabla \cdot \left(\rho \tilde{\mathbf{U}} \tilde{c}\right) - \nabla \cdot \left(\mu_t \nabla \tilde{c}\right) = \rho_u I_0 \tilde{s}_{u,lam} \Sigma \tag{19}$$

First, in order to simulate the *laminar-only* flame evolution, the source term of Eq. 19 depends only on the Σ distribution imposed by the Lagrangian ignition model (Eq. 18). Then, when the first channel diameter d_{spk} exceeds the threshold value of 2.5 *mm*, it is assumed that a *laminar-to-turbulent* flame transition is possible. Hence, the following transport equation for the flame surface density Σ starts to be solved [42, 43, 37]

$$\begin{aligned} &\frac{\partial \rho \tilde{\Sigma}}{\partial t} + \nabla \cdot \left(\rho \tilde{\mathbf{U}} \tilde{\Sigma}\right) - \nabla \cdot \left(\mu_t \nabla \left[\frac{(\rho \Sigma)}{\rho} \right] \right) \\ &+ \left(\nabla \cdot \tilde{\mathbf{U}}\right) \rho \Sigma = S \rho \Sigma - D \rho \Sigma^2 \end{aligned} \tag{20}$$

still considering the electrical circuit effects (Eq. 18) imposed on cells occupied by any spark-channel (both sustained and restriked ones). In Eq. 20, the source S and destruction D terms are modelled following Choi-Huh strategy [37]

$$\begin{cases} S = \alpha \left(u' / l_{tc}\right) \\ D = \beta \left\{ \left(I_0 s_{u,lam}\right) / \left[c\left(1-c\right) \right] \right\} \end{cases} \tag{21}$$

where α and β are model constant that need a proper calibration. In this work, their value is assumed as $\alpha = 0.5$ and $\beta = 0.1$. Finally, when the *fully turbulent* flame is self-sustained and departs from the ignition region, the Lagrangian particle contribution vanishes. As a consequence, it is assumed that when a channel diameter d_{spk} reaches a reasonable high value (5 *mm*), its particles can be removed.

Assessment on a Research SI Engine

Experimental and Numerical Setup

A pent-roof single-cylinder SI engine, characterized by a compression ratio of $CR = 12$, a stroke to bore ratio of 1.3 and a premixed Isoocatane-Air mixture, was selected for the assessment of the proposed numerical approach. At fixed engine and mixture conditions, the performances of two different ignition systems were investigated. A *classical* coil (Case 02), characterized by the well-known triangular shaped current profile [16], is compared to an *enhanced* coil (Case 01), able to generate a higher starting secondary circuit current $i_{S,0}$ and maintaining its value for a user-defined duration [16]. The features of the two selected conditions are reported in Table 1, where the spark-advance is the same and equal to SA = -29 CAD. For the sake of clarity, in this work the Crank Angle Degrees (CAD) are always expressed considering the compression Top Dead Center (TDC) as 0 CAD.

Numerical simulations were carried out with Lib-ICE, which is a set of solvers and libraries based on the OpenFOAM® open-source platform and where the proposed numerical models were implemented. Transport equations of mass, momentum and chemical species were solved with the RANS approach and the k - ε model was used for turbulence.

Full cycle simulations were performed to achieve a realistic in-cylinder flow field at spark-timing. A schematic of the in-cylinder tumble motion features is reported in Figure 2, while flow field details near the spark-plug are reported in Figure 3, where a region of high flow velocity and turbulence intensity can be observed.

TABLE 1 Engine and coil parameters of the investigated conditions: *enhanched* coil (Case 01) vs. *classical* coil (Case 02) (ϕ: equivalence ratio; $i_{S,0}$: starting secondary circuit current (after breakdown stage); $\Delta t_{iS,0}$: time-duration in which $i_{S,0}$ is maintained constant; ω: engine rotational speed.)

Case	ϕ [-]	$i_{S,0}$ [mA]	$\Delta_{tiS,0}$[ms]	ω [rpm]
01	0.58	120	1	1200
02	0.58	80	0	1200

FIGURE 2 Cylinder-head geometry and main flow features during compression stage: y-normal plane clip.

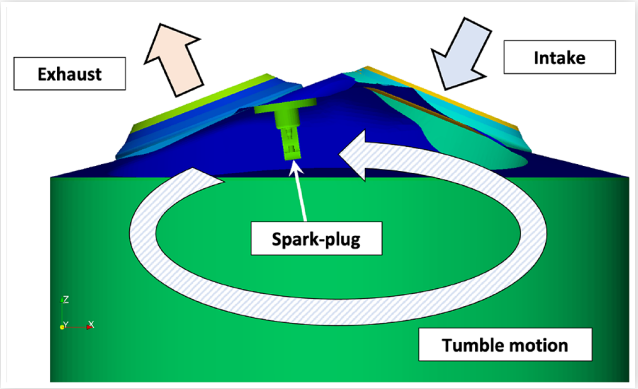

FIGURE 3 Cold-flow initial conditions at spark-timing (-29 CAD). (top figure) flow velocity **U** field; (bottom figure) turbulence intensity u' field.

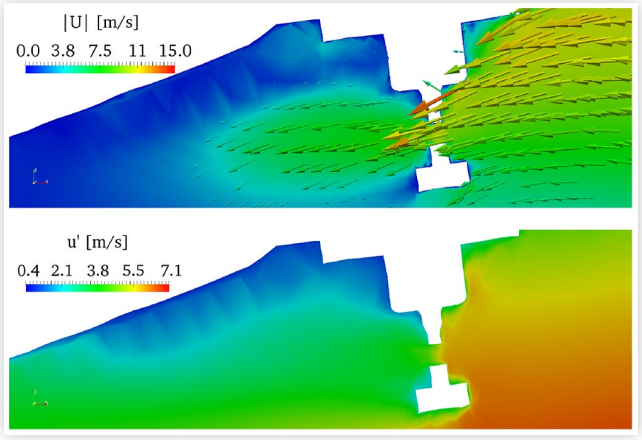

FIGURE 4 In-cylinder mesh structure at spark-timing (-29 CAD).

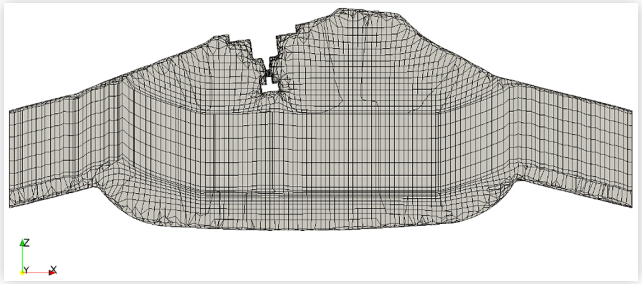

A slice on a y-normal plane of the 3-D computational mesh used for combustion simulations is shown by Figure 4. The mean grid size is around 0.6 mm and the number of cells goes from a minimum value of 260k (TDC) to a maximum of 470k (60 CAD). The dynamic layering technique was employed to accommodate the piston motion and preserve optimal mesh size in the combustion chamber [45]. The selected rather coarse grid comes from a trade-off between the achievement of reliable results with low computational costs. This choice is justified by the target of this work, which is a preliminary assessment of the proposed methodology for predicting the spark-discharge CCV using a CFD RANS approach.

Results and Discussion

Numerical simulations of 20 independent *single-cycle spark-discharges* were carried out for each investigated condition (Cases 01 and 02 of Table 1), starting from the same RANS

cold-flow fields (average conditions) at spark-advance. For each simulation:

- a random perturbed initial velocity was estimated for the channel particles, according to Eq. 1;
- a different *initial seed* was used for the prediction of η_i values (Eq. 4), to simulate a non-replicable random walk of the considered channel.

The numerical results, in terms of pressure p, apparent heat release rate AHRR, secondary current i_S and inter-electrode voltage V_{IE}, are shown by Figures 5 and 6, for both Cases 01 (left columns) and 02 (right columns). For clarity reasons, only 10 computed single-cycles are here represented (red lines) and compared with the experimental average behaviour over 200 measured power-cycles (black lines). Also the related maximum and minimum limits, in which measurements are distributed, are shown.

As it can be observed from pressure and AHRR traces of the simulated random discharges (Figure 5), there is a qualitatively wider distribution of results achieved for Case 02 (right column) if compared to Case 01 simulations (left column). Therefore, from a first rough estimation, an increase of the CCV is detected if a traditional coil (Case 02) is used instead of an enhanced one (Case 01). A possible explanation of this effect can rely on the higher sustain provided by the electrical circuit of Case 01 to the sparkdischarge, if compared

FIGURE 5 Computed pressure trends (top row), the related AHRR profiles (bottom row, solid lines) and the secondary current evolution (bottom row, dashed lines), for Cases 01 (left column) and 02 (right column). Results comes from 10 random initial perturbations $\mathbf{U}_{rnd}$ of channel particles velocity. The experimental average behaviour over 200 measured power-cycles is reported for all magnitudes with black lines. For pressures, also the envelope of maximum and minimum values for each crank angle is represented.

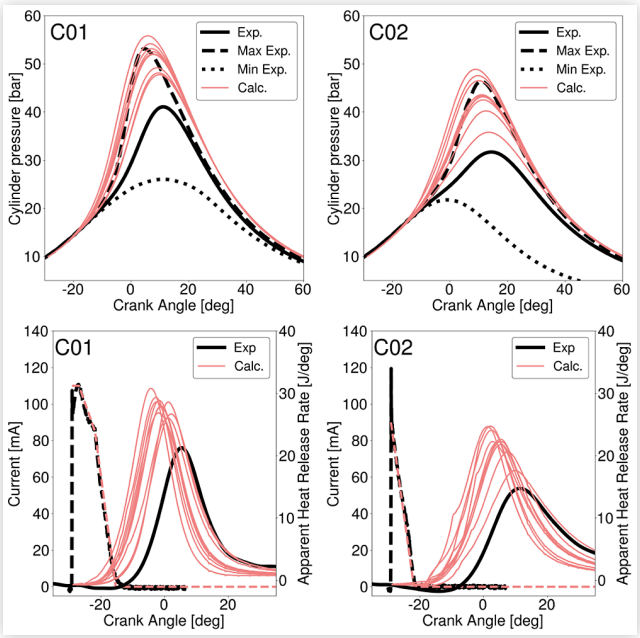

FIGURE 6 Computed secondary current trends (top row) and the related inter-electrode voltage profiles (bottom row) for Cases 01 (left column) and 02 (right column). Results comes from 10 random initial perturbations $\mathbf{U}_{rnd}$ of channel particles velocity. The experimental average behaviour over 200 measured power-cycles is reported for all magnitudes with black lines, as well as the envelope of maximum and minimum values for each crank angle.

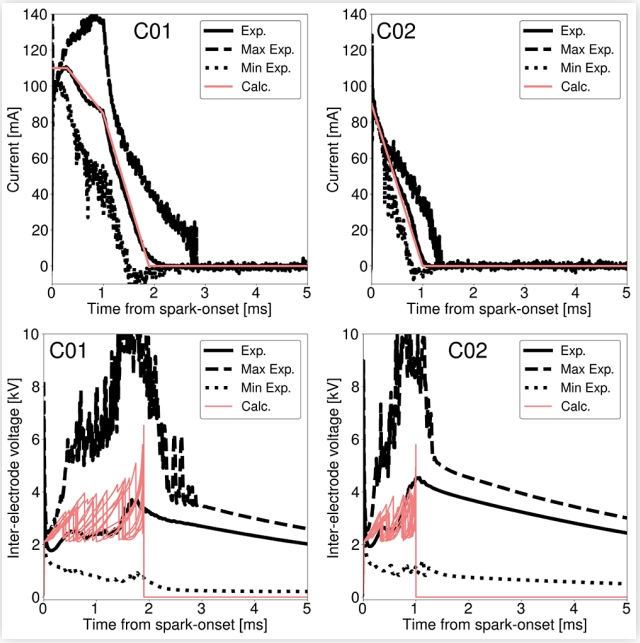

to the classical coil behaviour. In fact, a longer discharge characterized also by higher values of current (Figure 6, top row) seems able to generate high inter-electrode voltages for longer time durations (Figure 6, bottom row), hence longer sustained spark-channels (see Eq. 15). The consequent greater amount of thermal energy introduced by the electrical circuit of Case 01, with respect to Case 02 one, seems to allow the generation of a fully-turbulent flame before the discharge completion, at least for the majority of the computed single-discharge events (Figure 5, bottom-left chart). This seems not happening for the traditional coil (Figure 5, bottom-right chart), where a higher ignition-delay is qualitatively observable.

To get more insight in the capabilities of the proposed methodology, Figure 7 shows a quantitative comparison between the measured indicated mean effective pressure (IMEP) and its coefficient of variation (CoV) over 200 experimental power-cycles (dashed lines), with the variation of the same computed magnitudes (solid lines) as function of the considered numerical single-cycle discharges. As it can be observed from the right chart, the proposed numerical approach shows promising results in predicting the ignition system effects on the combustion CCV. In fact, the experimental trend of a lower CCV if an enhanced coil is used in place of a classical one (from Case 02 to Case 01) seems captured, despite the few considered numerical cycles.

Nevertheless, few aspects need further investigations. First, the much higher IMEP predicted for both Cases 01 and 02 with respect to the experimental value (Figure 7, left chart),

FIGURE 7 Variation of computed (solid lines) values of IMEP (left chart) and its CoV (right chart) as function of the considered number of single-cycle discharges, compared to measured values (dashed lines) over 200 experimental cycles.

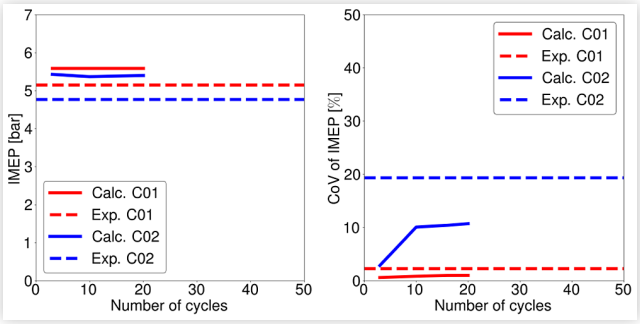

despite the measured trend seems captured. From a qualitative point of view, this aspect can be also observed in Figure 5, where all pressure traces seem centered on a higher average pressure profile than the experimental one, as well as the related numerical AHRR seem to be too anticipated. A possible reason of this behaviour could be related to the near-DNS prediction of each single-cycle spark-channel length, which is consequently always longer (because more corrugated) than the "average" channel evolution. As a consequence, more energy is introduced into the fresh mixture, producing an anticipated ignition. Therefore, the Lagrangian-Eulerian coupling needs probably to be improved to take into account this effect. Second, the impact on the combustion CCV provided by the fully-turbulent flame evolution inside a single-cycle 3D flow field is clearly not considered, because all Eulerian fields are evolved according to flow average conditions (RANS). Despite this topic is out of the scope of this work, a quantitative estimation of this effect needs to be provided to achieve a complete and reliable prediction of the combustion CCV of a SI engine. Third, the present assessment was carried out by imposing the experimental average current trend (Figure 6, top row) for modelling the electrical circuit features. Hence, fluctuations of the secondary current are not taken into account. This, probably, could affect the inter-electrodes voltage trends, maybe generating wider fluctuations (Figure 6, bottom row). Therefore, an investigation of the effect produced by imposing the energy stored into the secondary circuit instead of the current discharge profile should be considered.

Finally, Figures 8 and 9 allow to visualize, for a single-discharge event of Cases 01 and 02, the 3-D behaviour of the Lagrangian ignition model and its coupling with the Eulerian turbulent flame development, respectively. This last aspect is represented through a $c = 0.8$ iso-surface, which identifies the evolution of the almost fully burned mixture volume; to be precise, of the 3-D region where the probability to find burned gases is higher than 80%. For consistency reasons, similar (in terms of magnitude) perturbed initial velocities of the spark-channel are considered from Cases 01 (top row of each box figure) and 02 (bottom row of each box figure). Starting from -28 CAD, when both discharges have similar behaviours (only 1 CAD after spark-advance), the enhanced

FIGURE 8 Evolution of a simulated electrically-sustained sparkchannel (particles marked with bigger black squares and a more intense colour) and all its restriked portions (particles marked with smaller black squares and a less intense colour) from -28 CAD (top figure) to -10 CAD (bottom figure). In each figure (black box) are compared results from Case 01, perturbation of +86.15 % (top row), and Case 02, perturbation of +82.67 % (bottom row), over *y*-normal (left column) and *z*-normal (right column) planes.

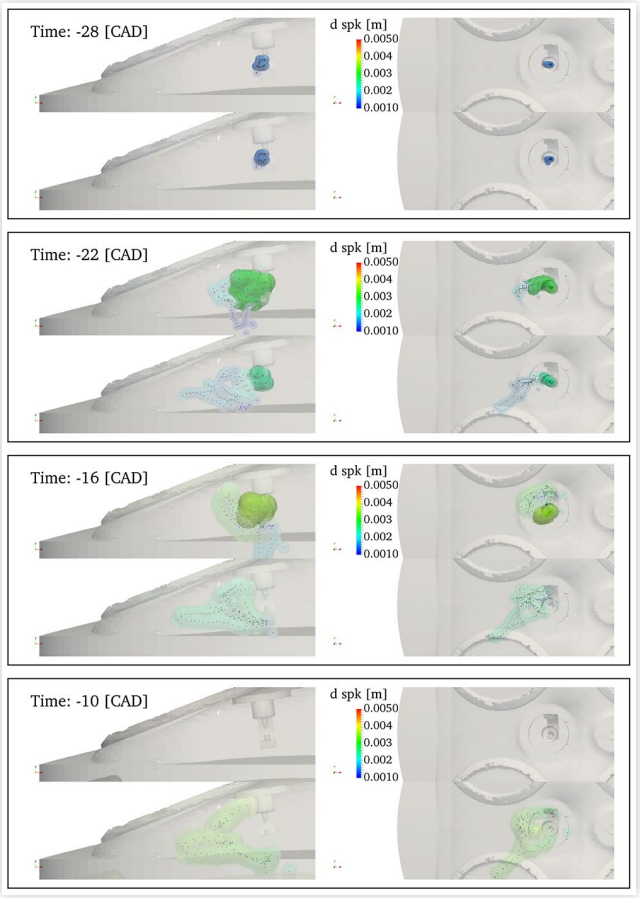

coil shows higher capabilities in sustaining longer arcs, hence igniting a wider mixture region, as time progresses. This can be observed at -22 CAD, when the classical coil is almost at its discharge end, with the burned region mainly overlapped to previous restrikes.

At the same time, the enhanced ignition system is still able to sustain a long and corrugated arc, which seems to control the burned mixture region. The discrepancy between the two investigated ignition systems increases at -16 and -10 CAD. With the enhanced coil, a fully-turbulent self-sustained flame seems to develop close to the discharge end. In fact, at -10 CAD all Lagrangian particles are removed, because the mixture is completely burned close to spark-plug region. The classical coil, instead, shows an appreciable ignition delay, because the early flame propagation seem more controlled by restriked channels.

FIGURE 9 Evolution of the mixture ignition process from -28 CAD (top figure) to -10 CAD (bottom figure), where the red cloud represents a c = 0.8 iso-surface. In each figure (black box) are compared results from Case 01, perturbation of +86.15 % (top row), and Case 02, perturbation of +82.67 % (bottom row), over y-normal (left column) and z-normal (right column) planes. Also the simulated electrically-sustained spark-channel and all its restriked portions (already shown in Figure 8) are included.

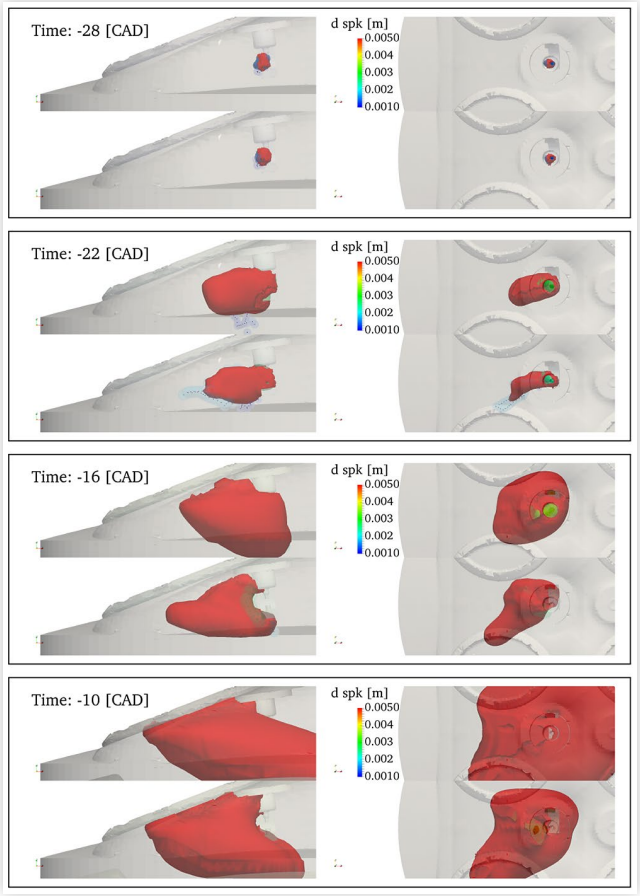

Conclusions

A numerical model is proposed to predict the impact of the ignition system features on the combustion CCV of SI engines. The methodology is based on a Lagrangian description of the spark-channel evolution, including restrikes modelling and early laminar flame development, coupled with an Eulerian approach for the propagation of the fully-turbulent self-sustained flame. Starting from RANS average flow conditions, first, the particles velocity is modified at spark-advance, with an homogeneous and zero-divergence perturbation. Then, each channel is evolved according to the Simplified Langevin Model (SLM), which keeps memory of the initial perturbation and simulates a random walk of the particles in the velocity space, due to stochastic interactions (Wiener process). A preliminary assessment of the proposed modelling approach was carried out on a pent-roof high-tumble single-cylinder SI engine, run with an ultra-lean premixed Isooctane-Air mixture. At fixed engine conditions, two different ignition systems were investigated: a classical coil, characterized by the well-known triangular shaped current profile, and an enhanced coil, able to generate higher currents for a user-defined durations. After the simulation of 20 independent single-cycle spark-discharges, the proposed model seems able to qualitatively estimate the increase of the comustion CCV, as well as the IMEP reduction, observed from experimental measurements over 200 power-cycles when the classical coil is used in place of the enhanced one. Some aspects need further investigations, such as: the overprediction of the IMEP on both conditions, the not-considered impact on combustion CCV of the fully-turbulent flame propagation on single-cycle conditions, and the effect produced by the fluctuations of the secondary current. Nevertheless, the proposed methodology seems very promising to provide a fast and reliable preliminary estimation of the impact produced by the ignition system features on the combustion stability of new generation SI engines, operated at part-loads.

References

1. Guido, C., Napolitano, P., Alfuso, S., Corsetti, C. et al., "How Engine Design Improvement Impacts on Particle Emissions from an HD SI Natural Gas Engine," *Energy* (2021).
2. Liu, Z., Sun, P., Du, Y., Yu, X. et al., "Improvement of Combustion and Emission by Combined Combustion of Ethanol Premix and Gasoline Direct Injection in SI Engine," *Fuel* 292 (2021): 120403.
3. Atis, C., Huisjen, A., Hardman, K., and Schock, H., "Experimental Investigation on the Effects of Design and Control Factors on the Performance and Emissions Characteristics of a Boosted GDI Engine Using Taguchi Method," in *SAE WCX Digital Summit*, SAE International, Apr 2021.
4. Bunce, M., Peters, N., Subramanyam, S.K.P., Blaxill, H. et al., "The Impact of Advanced Fuels and Lubricants on Thermal Efficiency in a Highly Dilute Engine," in *SAE WCX Digital Summit*," SAE International, Apr 2021.
5. Solomon, A., Battiston, P., and Sczomak, D., "Lean-Stratified Combustion System with Miller Cycle for Downsized Boosted Application-Part I," in *SAE WCX Digital Summit*, SAE International, Apr 2021.
6. Battiston, P., Wheeler, J., Solomon, A., and Sczomak, D., "Lean-Stratified Combustion System with Miller Cycle for Downsized Boosted Application - Part 2," in *SAE WCX Digital Summit*, SAE International, Apr 2021.
7. Göktaş, M., Balki, M.K., Sayin, C., and Canakci, M., "An Evaluation of the use of Alcohol Fuels in SI Engines in Terms of Performance, Emission and Combustion Characteristics: A Review," *Fuel* 286 (2021): 119425.
8. Lemazurier, L., Shidore, N., Kim, N., Moawad, A. et al., "Impact of Advanced Engine and Powertrain Technologies on Engine Operation and Fuel Consumption for Future Vehicles," SAE Technical Paper 2015-01-0978 (2015), https://doi.org/10.4271/2015-01-0978.

9. Blochum, S., Gadomski, B., Retzlaff, M., Thamm, F. et al., "Potential Analysis of a DMC/MeFo Mixture in a DISI Single and Multi-Cylinder Light Vehicle Gasoline Engine," in *SAE WCX Digital Summit*, SAE International, Apr 2021.
10. Falfari, S., Cazzoli, G., Ricci, M., and Forte, C., "PWI and DWI Systems in Modern GDI Engines: Optimization and Comparison Part I: Non-Reacting Flow Analysis," in *SAE WCX Digital Summit*, SAE International, Apr 2021.
11. Falfari, S., Bianchi, G.M., Pulga, L., and Forte, C., "PWI and DWI Systems in Modern GDI Engines: Optimization and Comparison Part II: Reacting Flow Analysis," in *SAE WCX Digital Summit*, SAE International, Apr 2021.
12. da Costa, R.B.R., Filho, F.A.R., Moreira, T.A.A., Baêta, J.G.C. et al., Exploring the Lean Limit Operation and Fuel Consumption Improvement of a Homogeneous Charge Pre-chamber Torch Ignition System in an SI Engine Fueled with a Gasoline-Bioethanol Blend. *Energy*,197:117300, 2020.
13. Singh, A., and Maurya, R.K., "Accessing the Predictabilities in Cyclic Combustion and Emission Variations in SI Engines for Their Modelling and Control: A Literature Review," in *SAE WCX Digital Summit*, SAE International, Apr 2021.
14. Chapman, E., Studzinski, W., Monroe, R., Tolou, A. et al., "Impact of Fuel Detergent Type and Concentration on the Rate and Severity of Stochastic Preignition in a Turbocharged Spark Ignition Direct Injection Gasoline Engine," in *SAE WCX Digital Summit*, SAE International, Apr 2021.
15. Yue, Z. and Som, S., "Fuel Property Effects on Knock Propensity and Thermal Efficiency in a Direct-Injection Spark-Ignition Engine," *Applied Energy* 281 (2021): 114221.
16. Shiraishi, T., Teraji, A., and Moriyoshi, Y., "The Effects of Ignition Environment and Discharge Waveform Characteristics on Spark Channel Formation and Relationship between the Discharge Parameters and the EGR Combustion Limit," *SAE Int. J. Engines* 9, no. 1 (2016): 171-178. https://doi.org/10.4271/2015-01-1895.
17. Lee, S., Ko, I., Kim, W., Song, S. et al., "Analysis of the Correlation between Flow and Combustion Characteristics in Spark-Ignited Engine," in *SAE WCX Digital Summit*, SAE International, Apr 2021.
18. Masuda, R., Sayama, S., Fuyuto, T., Nagaoka, M. et al., "Application of Models of Short Circuits and Blow-Outs of Spark Channels under High-Velocity Flow Conditions to Spark Ignition Simulation," *International Powertrains, Fuels Lubricants Meeting* (Sep 2018).
19. Sayama, S., Kinoshita, M., Mandokoro, Y., and Fuyuto, T., "Spark ignition and Early Flame Development of Lean Mixtures under High-Velocity Flow Conditions: An Experimental Study," *International Journal of Engine Research* 20, no. 2 (2019): 236-246.
20. Sayama, S., Kinoshita, M., Mandokoro, Y., Masuda, R. et al., Quantitative Optical Analysis and Modelling of Short Circuits and Blow-Outs of Spark Channels under High-Velocity Flow Conditions, in *International Powertrains, Fuels Lubricants Meeting*, SAE International, Sep 2018.
21. Yu, X., Leblanc, S., Liu, M., Tjong, J. et al., "Performance of Spark Energy Distribution Strategy on a Production Engine under Lean-Burn Conditions," in *SAE WCX Digital Summit*, SAE International, Apr 2021.
22. Refael, S. and Sher, E., "A Theoretical Study of the Ignition of a Reactive Medium by Means of an Electrical Discharge," *Combustion and Flame* 59, no. 1 (1985): 17-30.
23. Song, J., and Sunwoo, M., "A Modeling and Experimental Study of Initial Flame Kernel Development and Propagation in SI Engines," in *SAE 2000 World Congress*, SAE International, Mar 2000.
24. Zhu, X., Sforza, L., Ranadive, T., Zhang, A. et al., "Experimental and Numerical Study of Flame Kernel Formation Processes of Propane-Air Mixture in a Pressurized Combustion Vessel," *SAE Int. J. Engines* 9, no. 3 (2016): 1494-1511. https://doi.org/10.4271/2016-01-0696.
25. Sforza, L., Lucchini, T., Onorati, A., Zhu, X. et al., "Modeling Ignition and Premixed Combustion Including Flame Stretch Effects," in *WCX™ 17: SAE World Congress Experience*, SAE International, Mar 2017.
26. Haworth, D.C., "Progress in Probability Density Function Methods for Turbulent Reacting Flows," *Progress in Energy and Combustion Science* 36, no. 2 (2010): 168-259.
27. Taylor, H.M. and Karlin, S., *A Second Course in Stochastic Processes*, 2nd ed. (Academic Press, 1981)
28. Pope, S.B., "A Lagrangian Two-Time Probability Density Function Equation for Inhomogeneous Turbulent Flows," *Physics of Fluids* 26 (1983).
29. Haworth, D.C. and Pope, S.B., "A Pdf Modeling Study of Self-Similar Turbulent Free Shear Flows," *Physics of Fluids* 30 (1987).
30. Monin, A.S., Yaglom, A.M., and Lumley, J.L., *Statistical Fluid Mechanics: Mechanics of Turbulence*, 1st English ed. Vol. 2 (The MIT Press, 1975)
31. Obukhov, A.M., "Description of Turbulence in Terms of Lagrangian Variables," *Advances in Geophysics* 6 (1959): 113-116.
32. Anand, M.S. and Pope, S.B., "Diffusion Behind a Line Source in Grid Turbulence," in: Bradbury, L.J.S., Durst, F., Launder, B.E., Schmidt, F.W. et al. (Eds), *Turbulent Shear Flows 4*, (Berlin, Heidelberg: Springer Berlin Heidelberg, 1985), 46-61.
33. Sforza, L., Lucchini, T., Gianetti, G., and D'Errico, G., "Development and Validation of SI Combustion Models for Natural-Gas Heavy-Duty Engines," SAE Technical Paper 2019-24-0096 (2019), https://doi.org/10.4271/2019-24-0096.
34. Lucchini, T., Cornolti, L., Montenegro, G., D'Errico, G. et al., "A Comprehensive Model to Predict the Initial Stage of Combustion in SI Engines," SAE Technical Paper 2013-01-1087 (2013), https://doi.org/10.4271/2013-01-1087.
35. Gülder, Ö., "Correlations of Laminar Combustion Data for Alternative S.I. Engine Fuels," SAE Technical Paper 841000 (1984), https://doi.org/10.4271/841000.
36. Bray, K.N.C., "Studies of the Turbulent Burning Velocity," *Proceedings of the Royal Society of London Series A* (1990): 315-335.
37. Choi, C.R. and Huh, K.Y., "Development of a coherent flamelet Model for a Spark-Ignited Turbulent Premixed Flame in a Closed Vessel," *Combustion and Flame* 114, no. 3-4 (Aug 1998): 336-348.
38. Kim, J., and Anderson, R.W., "Spark Anemometry of Bulk Gas Velocity at the Plug Gap of a Firing Engine," in *1995 SAE International Fall Fuels and Lubricants Meeting and Exhibition*, SAE International, Oct 1995.

39. Herweg, R. and Maly, R., "A Fundamental Model for Flame Kernel Formation in S. I. Engines," SAE Technical Paper 922243 (1992), https://doi.org/10.4271/922243.
40. Pashley, N., Stone, R., and Roberts, G., "Ignition System Measurement Techniques and Correlations for Breakdown and Arc Voltages and Currents," in *SAE 2000 World Congress*, SAE International, Mar 2000.
41. Marble, F.E. and Broadwell, J.E., *The Coherent Flame Model for Turbulent Chemical Reactions* (TRW Defense and Space Systems Group: Technical report, 1977)
42. Duclos, J.M., Veynante, D., and Poinsot, T., "A Comparison of Flamelet Models for Premixed Turbulent Combustion," *Combustion and Flame* 95, no. 1-2 (Oct 1993): 101-117.
43. Prasad, R.O.S. and Gore, J.P., "An Evaluation of Flame Surface Density Models for Turbulent Premixed Jet Flames," *Combustion and Flame* 116, no. 1-2 (Jan 1999): 1-14.
44. Veynante, D., Piana, J., Duclos, J.M., and Martel, C., "Experimental Analysis of Flame Surface Density Models for Premixed Turbulent Combustion," *Symposium (International) on Combustion* 26, no. 1 (Jan 1996): 413-420.
45. Lucchini, T., Della Torre, A., D'Errico, G., Montenegro, G. et al., "Automatic Mesh Generation for CFD Simulations of Direct-Injection Engines," SAE Technical Paper 2015-01-0376 (2015), https://doi.org/10.4271/2015-01-0376.

ISSN 0148-7191